

Synthesis and Biological Studies of Pyrazolyl-Diamine Pt^{II} Complexes Containing Polyaromatic DNA-Binding Groups

Sofia Gama,^[a] Filipa Mendes,^[a] Teresa Esteves,^[a] Fernanda Marques,^[a] António Matos,^[b] José Rino,^[c] Joana Coimbra,^[d] Mauro Ravera,^[e] Elisabetta Gabano,^[e] Isabel Santos,^[a] and António Paulo^{*[a]}

New [PtCl(pz*NN)]²⁺ complexes anchored by pyrazolyl-diamine (pz*NN) ligands incorporating anthracenyl or acridine orange DNA-binding groups have been synthesized so as to obtain compounds that would display synergistic effects between platination and intercalation of DNA. Study of their interaction with supercoiled DNA indicated that the anthracenyl-containing complex L²Pt displays a covalent type of binding, whereas the acridine orange counterpart L³Pt shows a combination of intercalative and covalent binding modes with a strong contribution from the former. L²Pt showed a very strong cytotoxic effect on ovarian carcinoma cell lines A2780 and A2780cisR, which are, respectively, sensitive to and resistant to cisplatin. In these cell lines, L²Pt is nine to 27 times more cytotoxic than cisplatin. In the sensitive cell line, L³Pt showed a cytotoxic ac-

tivity similar to that of cisplatin, but like L²Pt was able significantly to overcome cisplatin cross-resistance. Cell-uptake studies showed that L²Pt accumulates preferentially in the cytoplasm, whereas L³Pt reaches the cell nucleus more easily, as clearly visualized by time-lapse confocal imaging of live A2870 cells. Altogether, these findings seem to indicate that interaction with biological targets other than DNA might be involved in the mechanism of action of L²Pt because this compound, despite having a weaker ability to target the cell nucleus than L³Pt, as well as an inferior DNA affinity, is nevertheless more cytotoxic. Furthermore, ultrastructural studies of A2870 cells exposed to L²Pt and L³Pt revealed that these complexes induce different alterations in cell morphology, thus indicating the involvement of different modes of action in cell death.

Introduction

Cisplatin [*cis*-DDP, *cis*-diamminedichloroplatinum(II)] has a central role in cancer chemotherapy, being the most widely used platinum-based anticancer drug. It is currently prescribed in the treatment of bladder, ovarian, cervical, head and neck, non-small-cell lung, and other cancers, being curative in nearly all cases of testicular cancer.^[1–2] Although cisplatin can induce apoptosis in cancer cells through binding to DNA, the drug also undergoes many non-selective reactions with a variety of biomolecules, such as proteins and phospholipids. Furthermore, the drug is rapidly distributed throughout the whole body upon administration, interacting both with healthy and with cancerous tissues.^[3] Treatment is thus limited by the side effects of nephrotoxicity, emetogenesis, and neurotoxicity.^[1]

To overcome these drawbacks it is fundamental to understand the mechanism of action of cisplatin and, probably even more importantly, the mechanisms by which cells process cisplatin.

The major cellular processes by which cisplatin enters and damages cancer cells include uptake and transport, formation of DNA adducts and their recognition by damage-response proteins, and signal transduction leading to cell-cycle arrest, repair, and/or death. Any factor that interferes with these pathways can lead to drug resistance.^[1]

With the aim of circumventing cisplatin's toxicity and drug resistance, new and selective anti-tumoral platinum compounds have been pursued. One of the strategies envisaged for the design of more selective platinum anticancer agents

has been the improvement of the formation of DNA adducts. This can be achieved by different approaches, such as regulating tumor-selective uptake and/or increasing the affinity of the drug to nuclear DNA through a DNA targeting approach.^[3–4] The rationale behind this approach is that the incorporation into the platinum complex of a functional group that will interact or intercalate with DNA might lead to an increase in the

[a] Dr. S. Gama, Dr. F. Mendes, Dr. T. Esteves, Dr. F. Marques, Dr. I. Santos, Dr. A. Paulo
Instituto Superior Técnico, Instituto Tecnológico e Nuclear
Unidade de Ciências Químicas e Radiofarmacêuticas
Estrada Nacional 10, 2686-953 Sacavém (Portugal)
E-mail: apaulo@itn.pt

[b] Dr. A. Matos
Centro Hospitalar de Lisboa Central Hospital Curry Cabral
Serviço de Anatomia Patológica
R. da Beneficência 8 1069-166 Lisboa (Portugal)

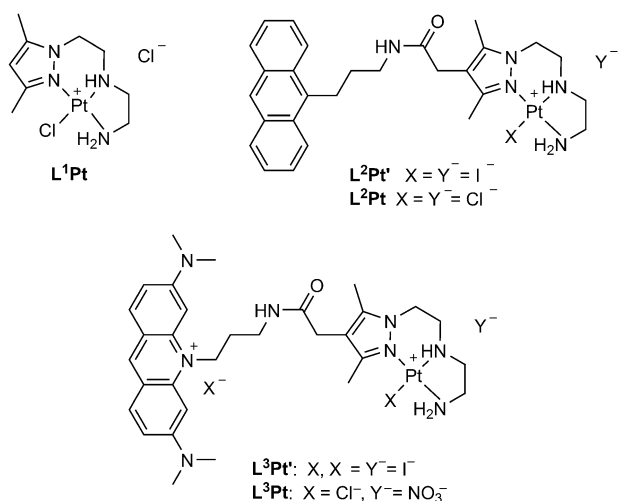
[c] Dr. J. Rino
Faculdade de Medicina da Universidade de Lisboa–
Instituto Medicina Molecular
Av. Prof. Egas Moniz, 1649-028 Lisboa (Portugal)

[d] Dr. J. Coimbra
Universidade de Aveiro, Laboratório Central de Análises
Campo de Santiago 3810-193 Aveiro Campus de Santiago
Aveiro (Portugal)

[e] Dr. M. Ravera, Dr. E. Gabano
Dipartimento di Scienze e Innovazione Tecnologica
Università del Piemonte Orientale "Amedeo Avogadro"
Viale Michel 11, 15100, Alessandria (Italy)

rate and extent of localization of the platinum in the vicinity of its DNA target. This proximity might in turn decrease the number of side reactions and probably enhance the interaction of the platinum compound with the nucleobases. In accordance with this strategy, different platinum complexes incorporating DNA intercalators in their structures have been developed and studied.^[5–6] So far, the platinum-intercalator technology has resulted in derivatives that are approximately 500 times more potent than cisplatin in chemoresistant cancers.^[4]

Our group has previously reported a small series of Pt^{II} complexes containing bidentate (pz*N) and tridentate (pz*NN) pyrazolylalkylamine chelators. In the particular case of a monochlorido Pt^{II} complex with the tridentate chelator *N*'-(2-(3,5-dimethyl-1*H*-pyrazol-1-yl)ethyl)ethane-1,2-diamine (**L¹Pt**, Scheme 1), DNA interaction studies showed that this complex forms monofunctional adducts and, consistently, is less active



Scheme 1. Pt complexes **L¹Pt**, **L²Pt**, **L²Pt**, **L³Pt**, and **L³Pt** with tridentate pz*NN ligands **L¹**, **L²**, and **L³**.

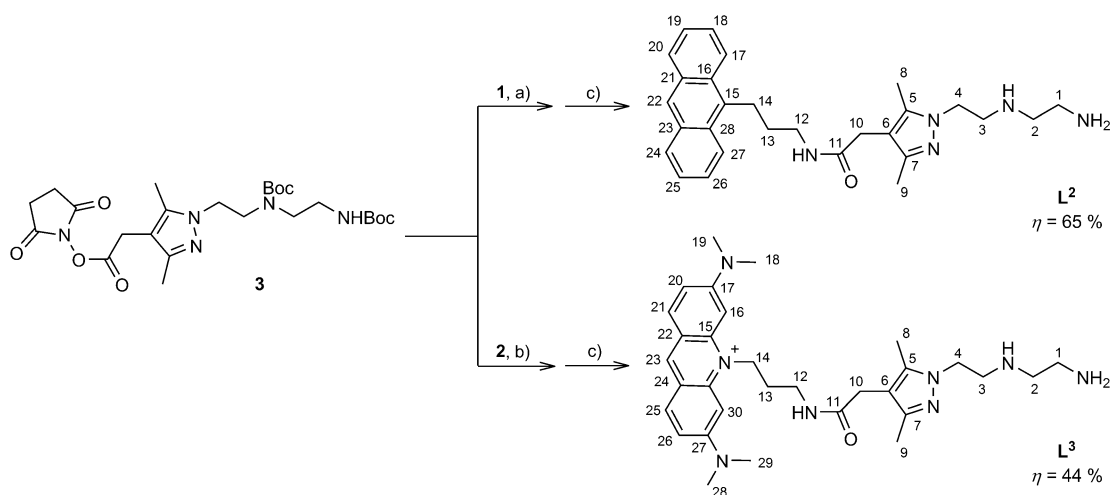
than cisplatin on the ovarian carcinoma A2780 cell line. Nevertheless, its activity in the cisplatin-resistant A2780cisR cell line is significantly retained, so **L¹Pt** presented a lower resistance factor than cisplatin.^[7]

Moreover, we have also shown that ^{99m}Tc^I tricarbonyl complexes anchored by pyrazolyl-diamine ligands functionalized with polyaromatic DNA intercalators have the ability to target the nuclei of tumor cells, with some complexes causing significant cell killing at low radioactivity levels, mainly through apoptotic pathways.^[8–10] These encouraging results prompted us to study Pt^{II} complexes anchored by pyrazolyl-diamine chelators bearing planar and aromatic DNA-intercalating groups. Our main goal was to obtain compounds that would display a synergistic effect between platination and intercalation of DNA. To achieve such a goal, we have synthesized two new Pt^{II} complexes anchored by pyrazolyl-diamine ligands bearing anthracenyl (**L²Pt**) or acridine orange (**L³Pt**) as DNA-binding groups. Here we report on the synthesis and characterization of **L²Pt** and **L³Pt** and on their in vitro evaluation, which consisted of study of their interaction with plasmid DNA, cytotoxicity assays against cisplatin-sensitive and -resistant ovarian cancer cell lines, Pt^{II} uptake measurements, and ultrastructural analysis in the same cell lines. For the purposes of comparison, some of these in vitro studies were also performed with **L¹Pt**,^[7] which is stabilized by the same pyrazolyl-diamine chelating structure but without DNA-intercalating groups.

Results and Discussion

Synthesis and characterization of the ligands and corresponding Pt^{II} complexes

The two pyrazolyl-diamine chelators **L²** and **L³** (Scheme 2)—bearing anthracenyl and acridine orange (AO) intercalating moieties, respectively, at the 4-positions of their pyrazolyl rings—were synthesized by the methodology for related ligands previously reported by our group.^[10] As depicted in



Scheme 2. Synthesis of chelators **L²** and **L³**. The numbering schemes are those used to identify the ¹H and ¹³C NMR signals for the ligands and the corresponding Pt^{II} complexes. a) Dry CH₂Cl₂, DIPEA, RT, 48 h; b) DMF, DIPEA, RT, 91 h; c) HCl, MeOH, RT, 24 h.

Scheme 2, the synthesis of **L**² and **L**³ consisted of treatment either of 9-(3-aminopropyl)anthracene (**1**) or of 10-(3-aminopropyl)-3,6-bis(dimethylamino)acridinium (**2**) with an activated ester (*N*-hydroxysuccinimide, NHS) of BOC-protected pyrazolyl-diamine derivative **3**. Compounds **1** and **3** were synthesized by the methods described in the literature^[11–15] and compound **2** was prepared from the commercially available acridine orange by the methodology that we had used previously for the butyric congener.^[10] After removal of the BOC protecting groups and appropriate workup, the final ligands **L**² and **L**³ were recovered in moderate yields (40–65%) as pale yellow and red solids, respectively. These two new compounds were characterized by mass spectrometry (ESI-MS) and multinuclear NMR spectroscopy (¹H and ¹³C).

The Pt^{II} complexes **L**²Pt and **L**³Pt (Scheme 1) were synthesized in water by procedures described in the literature with slight modifications,^[7,16–17] based on Dhara's method.^[18–20] Briefly, K₂[PtCl₄] (produced in solution by treatment of K₂[PtCl₄] with KI) was treated with the ligands to yield [Pt(pz*NN)]_n (**L**²Pt', *n* = 1; **L**³Pt', *n* = 2). Upon treatment of **L**²Pt' and **L**³Pt' with AgNO₃, the corresponding aqua intermediates [Pt(H₂O)(pz*NN)]ⁿ⁺ were formed, and treatment with KCl yielded the final chlorido complexes [PtCl(pz*NN)]ⁿ⁺ (**L**²Pt, *n* = 1; **L**³Pt, *n* = 2), which were obtained with mixtures of nitrate and chloride as counter ions, as confirmed by ion chromatography. The percentage of each counter ion present in each mixture was determined by ion chromatography. For **L**²Pt the obtained chromatograms indicated that chloride was the dominant counter ion (81%), with nitrate the remainder. To have a well-defined formulation of the final complex, the crude **L**²Pt was added to a suspension of anion-exchange resin in chloride form to replace the residual nitrate ions. In the case of **L**³Pt, in contrast, nitrate is practically the only counter ion present (ca. 98%), so no subsequent ion replacement step was performed. It is worth noting that the presence of different counter ions should not be expected to affect the cytotoxicities of complexes of this kind, as demonstrated for pyrazolyl-diamine Pt^{II} model complexes (e.g., **L**¹Pt, data not shown) not containing polyaromatic DNA binding groups.

The newly synthesized Pt^{II} complexes were characterized by ESI-MS and ¹H, ¹³C{¹H}, and ¹⁹⁵Pt{¹H} NMR spectroscopy. The ESI-MS spectra of the cationic Pt^{II} complexes **L**Pt' and **L**Pt (**L** = **L**², **L**³) showed peaks and isotopic patterns consistent with the expected molecular ions. In the corresponding ¹H and ¹³C spectra, the different signals were assigned by one- and two-dimensional, homo- and heteronuclear techniques, such as DEPT-135, ¹H,¹H COSY, and ¹H,¹³C HETCOR. It is particularly notable that the ¹H resonances due to the methylenic and pyrazolyl protons of the chelators are shifted downfield relative to the corresponding resonances of the corresponding free ligands, confirming the coordination of the azole rings and aliphatic amine groups of the chelators to the Pt^{II} metal center, as already reported for **L**¹Pt.^[7] In general, a coordinated ethylenediamine-like ligand adopts a *gauche* conformation conferring an approximately axial and equatorial character to each proton with respect to the plane of the metal ion and the nitrogen atoms.^[21–23] Moreover, the pz*NN ligands confer particu-

lar rigidity to the structure around the metal core (the conformation and the distortion of the coordinated pz*NN ligand can be observed in the X-ray structure of **L**¹Pt).^[7] It is therefore possible to distinguish different signals for the two protons (H_{4,ax} and H_{4,eq}) of the methylenic group near the azole ring: ¹H NMR spectra show one triplet at higher frequency for the axial proton and one doublet at lower frequency for the equatorial one, with these signals characterized by large geminal and axial–axial coupling constants. Such splitting has been observed previously for other rigid, although more symmetric, ethylenediamine-based ligands.^[24–25]

Well-defined multiplicity for both signals was observed here only for complex **L**²Pt in [D₆]acetone. In this case the signal of the axial proton looks like a triplet due to geminal and axial–axial coupling, with each line further split due to the axial–equatorial coupling (Figure 1). The signal for the equatorial

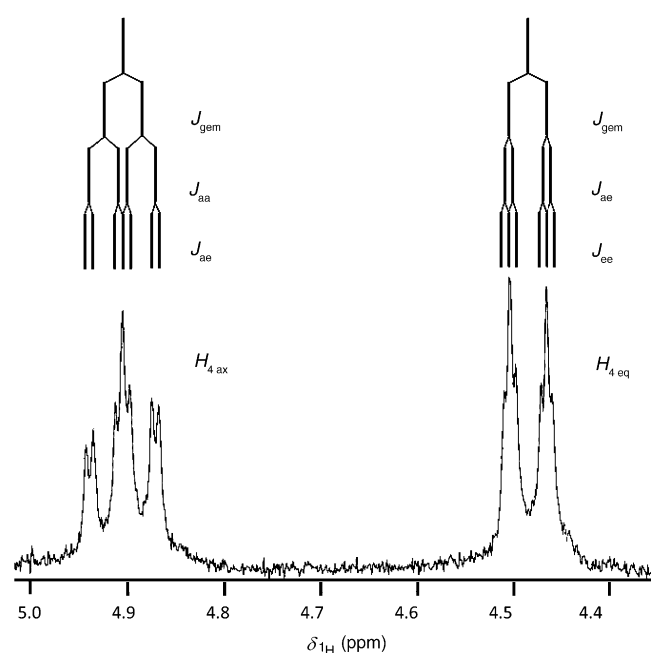


Figure 1. ¹H NMR spectrum of **L**²Pt in [D₆]acetone.

proton is a doublet, further split due to the axial–equatorial and equatorial–equatorial couplings;^[26] the distance between the two signals is $\Delta\delta = 0.43$ ppm. The coupling constants are generally related to the dihedral angle between the two coupled protons by the Karplus equation.^[22] The graphical tool MestReJ^[27] can predict vicinal proton–proton ³J_{H,H} coupling constants from the torsion angle between the coupled protons (and vice versa) for organic molecules through generalized Karplus equations such as the Haasnoot–de Leeuw–Altona equations.^[28] Applying this relation to the above coupling constants of **L**²Pt gives torsion angles of 187.4° (*J*_{aa}), 62.3° (*J*_{ae}), and 297.2° (*J*_{ee}). Even though comparison of the solid state with the properties of similar complexes (with the same coordination sphere) in solution is clearly rough, the calculated angles are close to agreement with the corresponding torsions in the X-ray structure of the model compound **L**¹Pt (185.0, 67.1 and 67.4, and 309.6°).^[7]

The ¹⁹⁵Pt{¹H} NMR spectra of freshly prepared solutions of complexes **L¹Pt** and **L²Pt** ($L=L^2, L^3$) each exhibited only one signal at chemical shifts consistent with the proposed coordination spheres, without involvement of solvation reactions. For the iodido complexes **L²Pt** and **L³Pt** these signals appear at -3113 and -3111 ppm, respectively, whereas in the case of the chlorido complexes **L²Pt** and **L³Pt** the corresponding ¹⁹⁵Pt chemical shifts are -2632 and -2655 ppm. These values are in very good agreement with those that we have reported for related pyrazolyl-diamine Pt^{II} complexes without DNA-binding groups (i.e., -3115 ppm and -2657 ppm for the "PtN₃" and "PtN₃Cl" cores, respectively).^[7]

Interaction with supercoiled DNA

The effects of the interaction of compounds **L²** and **L³** and the corresponding chloride Pt^{II} complexes (**L²Pt** and **L³Pt**) with supercoiled DNA were determined by the abilities of the compounds to modify the electrophoretic mobilities of the covalently closed circular (ccc) and open circular (oc) forms of ϕ X174 plasmid DNA. These studies were also used to assess the DNA unwinding angles (ϕ) induced by the **L²Pt** and **L³Pt** complexes. In a similar way, the same angles were also measured for the previously reported **L¹Pt**.^[7] Figure 2 shows the electrophoretic mobilities of native ϕ X174 plasmid DNA and ϕ X174 DNA incubated with different concentrations of these Pt^{II} complexes (**L¹Pt**, **L²Pt**, and **L³Pt**) and *cis*-DDP.

It is well known from the literature that a compound that unwinds the DNA double helix reduces the number of supercoils, with a consequent decrease in the superhelical density of closed circular DNA and a reduction in the rate of migration through the agarose gel.^[29] The increase in r_i , defined as the molar ratio of added platinum complex per nucleotide, decreases the rate of migration of ccc DNA until it comigrates with oc DNA. In this way a coalescence point [$r_i=r_b(c)$] corresponding to the amount of platinum needed

for complete removal of all supercoils from DNA is achieved.^[30]

As can be seen in Figure 2, the coalescent point for **L³Pt** is reached at a much lower r_i value (0.063) than for **L¹Pt** (value between 0.83 and 1.67), **L²Pt** (0.333), and even *cis*-DDP (0.161). This effect can be evaluated quantitatively by the DNA unwinding angle [ϕ] determined from the equation $\phi=18\sigma/r_b(c)$, where σ is the plasmid superhelical density and $r_b(c)$ is the molar ratio of platinum bound per nucleotide at the coalescence point, as described above. By using the unwinding angle of 13° previously reported for *cis*-DDP,^[29–33] a superhelical density of $\sigma=-0.116$ for supercoiled ϕ X174 plasmid DNA was determined. From this superhelical density we found the ϕ value for the AO-containing complex (**L³Pt**) to be approximately three times higher than that for *cis*-DDP (33 vs 13°). For complex **L²Pt** the obtained unwinding angle is 6° and for **L¹Pt** the ϕ value is around 2°.

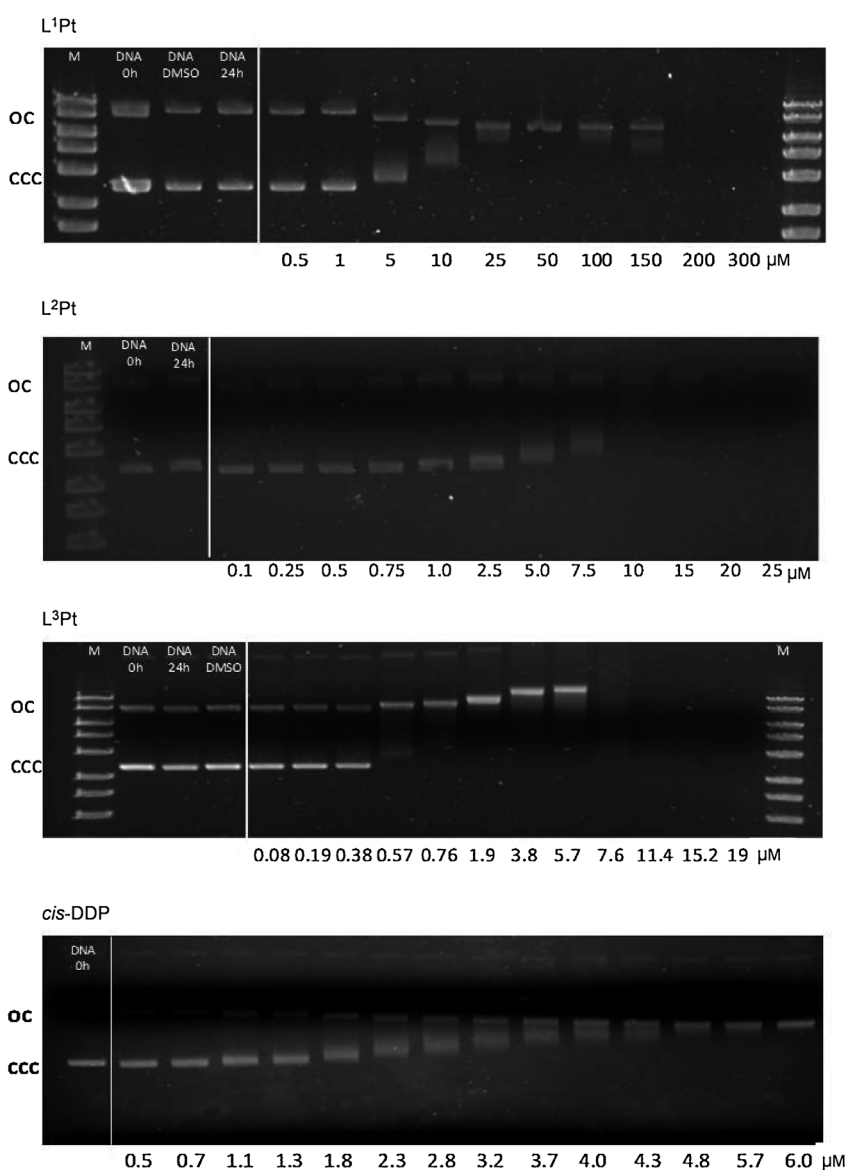


Figure 2. Interaction of supercoiled ϕ X174 DNA with **L¹Pt**, **L²Pt**, **L³Pt**, and *cis*-DDP after 24 h of incubation at 37 °C in phosphate buffer (pH 7.2). Forms ccc and oc are covalently closed circular and open circular, respectively, forms of DNA.

It would be expected that the interaction of L^1Pt with DNA should essentially involve DNA platination. Comparison of the ϕ values for L^1Pt and *cis*-DDP (2 vs 13°) confirmed that the platination of DNA by the former compound is much less efficient. The introduction of the anthracenyl polyaromatic ring seems to enhance the DNA interaction, as indicated by the increase in the unwinding angles from L^1Pt to L^2Pt (2 vs 6°). This trend might indicate a possible contribution of binding modes other than DNA platination, such as intercalative binding, for L^2Pt . Apparently this contribution is not very important, however, because the increase in the ϕ value is not that high. For the AO derivative L^3Pt , this increase is much higher, from 2 to 33°, and shows that the interaction effect probably involves a combination of intercalation/platination with a high contribution of DNA intercalation. The unwinding angle of L^3Pt is greater than that described for *cis*-DDP, which provides further evidence for a combined intercalation/covalent binding mode in the case of L^3Pt .

Experiments of the same type were run with the free ligands, to gain further insight into the interaction of the corresponding Pt^{II} complexes with DNA (Figure 3). In the case of the anthracene derivative L^2 , no effect on the DNA mobility was noted after 24 h of incubation. However, for the acridine orange ligand L^3 there was a change in the mobility of the plasmid DNA; this indicated that L^3 has a better ability than L^2 to interact with DNA. These findings are consistent with the results for L^2Pt and L^3Pt presented above: that is, a more probable contribution of the intercalation binding mode in the case of L^3Pt reflecting a higher DNA affinity for the AO chromophore than for anthracene.^[8,10]

The possible existence of a combined intercalation/platination effect was further studied in the presence of chloroquine.^[34] In these studies, L^2 and L^3 and the corresponding Pt^{II} complexes L^2Pt and L^3Pt were incubated with $\phi X174$ plasmid DNA at 37 °C for 24 h, with use of 5 μM concentrations ($r_1 = 0.17$) of the different tested compounds. The different mixtures were then analyzed by agarose gel electrophoresis in the presence of chloroquine (Figure 4).

Chloroquine induces positive supercoiling of plasmid DNA and promotes the resolution of topoisomeric forms of the plasmid: the slowest moving band of each lane represents the open circular DNA (oc form), whereas the other bands of each lane are all covalently closed circular DNA (ccc forms or topoisomers). Figure 4 shows that the bands of DNA topoisomers of the plasmid incubated with L^2 migrate similarly to those of

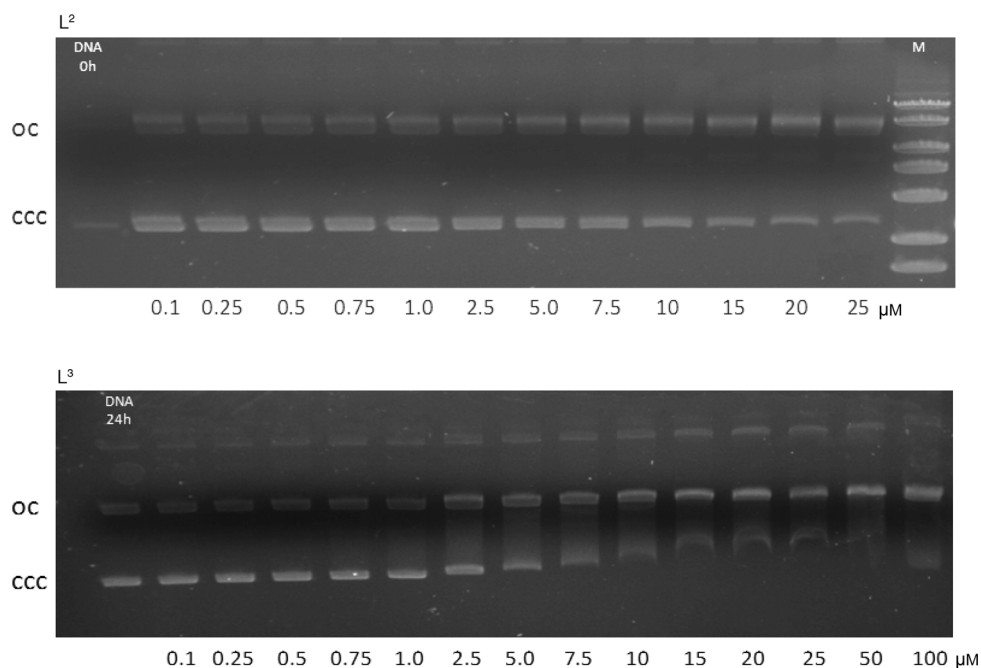


Figure 3. Interaction between supercoiled $\phi X174$ DNA and L^2 and L^3 after 24 h of incubation at 37 °C in phosphate buffer (pH 7.2).

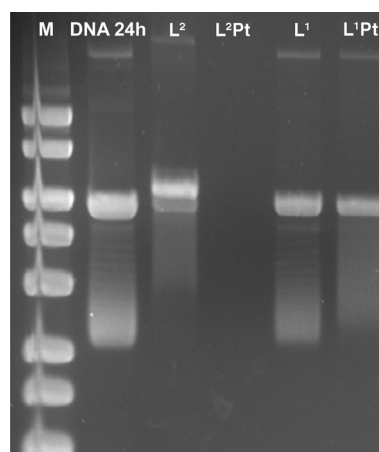


Figure 4. Resolution of DNA topoisomers of $\phi X174$ phage incubated with ligands (L^2 and L^3) and the corresponding Pt^{II} complexes (5 μM) for 24 h at 37 °C in phosphate buffer (pH 7.2), after agarose gel electrophoresis with chloroquine (1.25 $\mu g mL^{-1}$).

control plasmid in the presence of chloroquine. This indicates that $DNA \cdot L^2$ adducts are readily displaced by chloroquine. For L^2Pt , however, there is a slower migration, probably due the presence on the DNA of monofunctional adducts of platinum that are not displaced by chloroquine.

Ligand L^3 induces a much greater decrease in the mobilities of the topoisomers relative to the control, thus indicating that it negatively twists the supercoiled DNA. L^3 thus most likely acts as a strong intercalator, with chloroquine not being able to displace it easily from the DNA double helix. Unfortunately, the presence of a +2 charge on L^3Pt led to the migration of the sample in the opposite direction in the gel, preventing comparison with the control sample.

Taken together, the DNA interaction data obtained for **L²Pt** and **L³Pt** show that these two complexes have different DNA-binding abilities, with the contribution of the intercalating binding mode being more evident in the case of **L³Pt**.

Cytotoxic activity and cell uptake

To analyze the potentials of the complexes **L²Pt** and **L³Pt** as antitumor agents, their cytotoxic activities towards human epithelial ovarian carcinoma cells, both sensitive (A2780) and resistant (A2780cisR) to *cis*-DDP, were tested. For the purposes of comparison the cytotoxicities of *cis*-DDP, **L¹Pt**, and ligands **L¹**, **L²**, and **L³** were evaluated under the same experimental conditions. The ovarian cancer cells were treated with increasing concentrations of the different compounds for 24 and 72 h continuous incubation at 37 °C. With the exception of *cis*-DDP, which is water-soluble, all the tested compounds were first solubilized in DMSO and then diluted in the media for the cell studies. The percentage of DMSO never exceeded 1% and this concentration was without cytotoxic effect. After incubation, the cellular viability was determined by a MTT assay (MTT = 3-(4,5-dimethylthiazol-2-yl)-2,5-diphenyltetrazolium bromide). The viabilities of cells in the presence of the tested compounds were compared to that observed in controls (no drug) and the inhibitions of growth [%] were calculated. The IC₅₀ values were determined and are expressed in μM concentrations in Table 1.

As can be seen in Table 1, the anthracenyl derivatives **L²** and **L²Pt** each showed higher cytotoxic activity than the AO derivatives **L³** and **L³Pt** against both the sensitive and the resistant cell lines, and the Pt^{II} complexes were in general more cytotoxic than the corresponding ligands. **L²Pt** is a particularly active compound, exhibiting sub-micromolar IC₅₀ values (0.21–0.63 μM) in both cell lines after 72 h of incubation. Under these conditions, **L²Pt** showed a cytotoxic activity ten times higher than that of **L³Pt**, also being much more cytotoxic than *cis*-DDP. **L¹Pt** was not cytotoxic in the range of concentrations studied at 24 h incubation and displayed the highest IC₅₀ value at 72 h incubation. This shows that the presence of the polyaromatic DNA binding groups determines the cytotoxic activities of **L²Pt** and **L³Pt**. Nevertheless, the presence of the metal certainly plays an important role because **L²Pt** and **L³Pt** are more potent than the corresponding free ligands. Notably, both complexes can overcome cisplatin cross-resistance significantly,

with resistance factors ranging between 3.0 and 3.4 at 72 h of incubation, significantly lower than the value of 8.9 obtained for *cis*-DDP.

Compounds **L²Pt** and **L³Pt** can broadly be considered intramolecular fixed-dose-ratio combinations of their building blocks: **L²** or **L³** and **L¹Pt**. The effect of a combination of different drugs can be synergistic, additive, or antagonistic. Evaluation of the combined effects of the alkylating Pt moieties and their intercalating ligands was performed by comparing their cytotoxicity data through the combination index (CI) methodology. CI is a numerical value, obtained from the Chou–Talalay CI theorem, providing a quantitative measure of the extent of drug combination: CI = 1 means an additive effect, CI < 1 synergistic, and CI > 1 antagonistic (see the Experimental Section for further details).^[35–36] The CI values for compounds **L²Pt** and **L³Pt** were calculated for 50% residual viability after 72 h treatment according to the model of interaction for two mutually non-exclusive drugs. The CI values for 50% residual viability after 72 h treatment with compounds **L²Pt** and **L³Pt** indicated a synergic effect on both cell lines (CI < 0.05).

Cellular uptake studies were performed with ICP-MS analysis for quantification of the amounts of platinum in the cytoplasm and nuclear fractions of the ovarian cancer cells. Table 2 gives the cytoplasmic and nuclear Pt levels (expressed as ng of Pt per 10⁶ cells) found in both fractions for A2780 and A2780cisR cells after 3 h and 24 h exposure to **L¹Pt**, **L²Pt**, and **L³Pt** at equimolar concentrations (10 μM). For **L²Pt** it was not possible to determine Pt uptake after 24 h of incubation, due to the high cytotoxicity shown by the compound, which resulted in

Table 2. Platinum levels in A2780 and A2780cisR cell extracts after 3 h and 24 h complex exposure at 10 μM. Results are expressed as ng of Pt per 10⁶ cells.

		A2780 24 h	A2780 3 h	A2780cisR 3 h
L¹Pt	cyt ^[a]	3.3 ± 0.02	2.5 ± 0.06	4.1 ± 0.01
	nuc ^[a]	1.3 ± 0.01	0.38 ± 0.01	1.2 ± 0.04
L²Pt	cyt	–	15 ± 0.16	31 ± 0.1
	nuc	–	2.3 ± 0.01	4.9 ± 0.02
L³Pt	cyt	3.8 ± 0.06	1.2 ± 0.02	2.6 ± 0.05
	nuc	8.8 ± 0.4	1.5 ± 0.01	3.0 ± 0.09
<i>cis</i> -DDP	cyt	–	3.3 ± 0.06	–
	nuc	–	4.8 ± 0.18	–

[a] Cyt = cytoplasm and nuc = nucleus.

Table 1. IC₅₀ values for A2780 ovarian carcinoma cells and the cisplatin-resistant variant A2780cisR after 24 and 72 h of continuous treatment with compounds **L²**, **L³**, the corresponding Pt^{II} complexes (**L²Pt**, **L³Pt**), **L¹Pt**, and *cis*-DDP.

	IC ₅₀ [μM] 24 h		IC ₅₀ [μM] 72 h		RF ^[a]	
	A2780	A2780cisR	A2780	A2780cisR	24 h	72 h
L¹Pt	> 200	> 200	28.8 ± 5	44.9 ± 11	–	1.6
L²	13.3 ± 3	> 200	2.1 ± 0.7	4.5 ± 1.0	–	2.1
L²Pt	8.1 ± 3.8	12.9 ± 3.7	0.21 ± 0.8	0.63 ± 0.2	1.6	3.0
L³	150.5 ± 26	> 200	33.2 ± 6	47.6 ± 8	–	1.4
L³Pt	12.1 ± 1.7	28.7 ± 2.9	2.1 ± 0.6	7.3 ± 1.5	2.4	3.4
<i>cis</i> -DDP	36 ± 8	140 ± 40	1.9 ± 0.1	17.0 ± 3	3.9	8.9

[a] Resistance factor, defined as the ratio IC₅₀ A2780cisR/IC₅₀ A2780 cells.

no viable cells. For that reason, the studies for **L²Pt** were only performed at the shorter incubation time of 3 h.

After 3 and 24 h of incubation, the uptakes of **L¹Pt** and **L³Pt** in the cytoplasm of A2780 cells, in terms of platinum levels, are similar. However, the nuclear uptake is much higher in the case of the complex **L³Pt**, most probably due to the pres-

ence of the AO intercalator, which targets the DNA and carries the compound to the nucleus. After 3 h of incubation, complex L^2Pt is accumulated much more efficiently in the cell than L^1Pt , L^3Pt , or *cis*-DDP, as shown by the considerably higher total cellular Pt levels (sum of cytoplasm and nucleus) that were measured for L^2Pt . This finding probably justifies the low IC_{50} values measured for L^2Pt , although cellular uptake per se might not reflect the antitumor activities of the complexes.^[7,37] Importantly, nuclear internalization is comparatively higher for L^3Pt than for L^2Pt , corresponding to more than 50% of the total uptake in the case of L^3Pt and being roughly 13% of total uptake for L^2Pt . This intracellular distribution is consistent with the highest DNA affinity and intercalating ability of the L^3Pt complex, as discussed above.

The cellular trafficking of this compound was studied by time-lapse confocal fluorescence microscopy in live cells, by taking advantage of the fluorescent properties of L^3Pt . Cells were previously incubated with dihydroethidium (DHE) for whole-cell colocalization and imaged every minute for 30 min after addition of L^3Pt (100 μM) to the medium. As depicted in Figure 5, L^3Pt accumulates gradually in A2780 cells and targets the nucleus. Considerable accumulation of fluorescence in the nucleus is evident after 30 min incubation. Evaluation of the L^2Pt cellular trafficking was not possible, due to the particular excitation and emission characteristics of this compound (absorption/emission: 350/400 nm).

Ultrastructural analysis

To gain further insight on the mechanisms of action of L^2Pt and L^3Pt , the ultrastructures of A2780 cells exposed to these complexes were analyzed by TEM.

Representative images obtained for both compounds are shown in Figure 6. L^2Pt induced extensive necrotic changes with overall extraction of the cytoplasmic matrix contents and

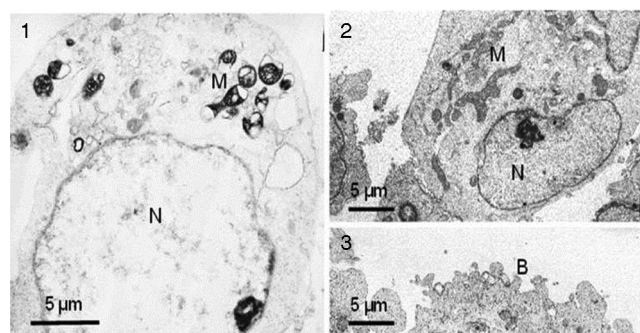


Figure 6. TEM images showing the ultrastructures of A2780 cells after treatment (20 μM , 2 h) with: 1) L^2Pt , and 2) and 3) L^3Pt . N: nucleus. M: mitochondria. B: surface blebs.

densification of the mitochondrial matrix (Figure 6.1). In addition, the organelles are often found clustering near the cell center, the nucleus edematous and the chromatin dispersed. In contrast, cells treated with L^3Pt presented much more conserved morphologies, with most cells having nearly normal ultrastructure (Figure 6.2). However, the mitochondria were enlarged and pleomorphic and no densification of the mitochondrial matrix was observed. Many cells displayed cytoplasmic blebs reminiscent of early morphologic stages of an apoptotic process (Figure 6.3).

Conclusions

New pyrazolyl-diamine Pt^{II} complexes containing anthracenyl or acridine orange groups for DNA binding have been synthesized and fully characterized. The anthracenyl derivative L^2Pt showed very strong cytotoxic effects on the ovarian carcinoma A2780 cell line, being about ten times more cytotoxic than the AO derivative L^3Pt and cisplatin. Nevertheless, both complexes

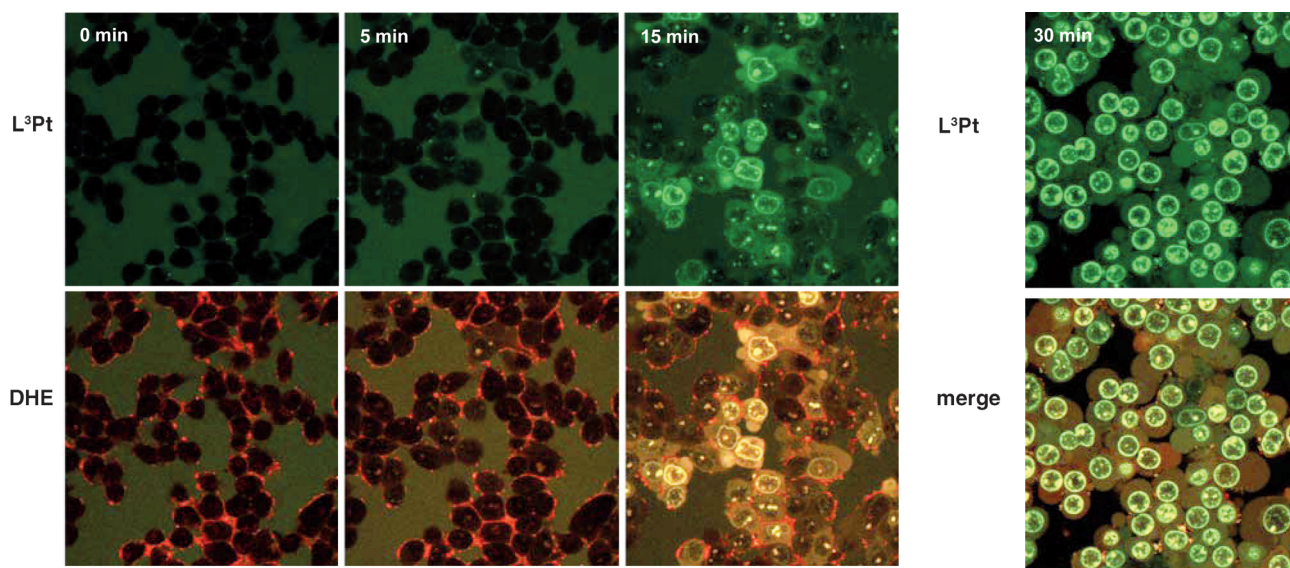


Figure 5. Live-cell uptake of L^3Pt by A2780 cells visualized by time-lapse confocal microscopy imaging. Cells were incubated with DHE for whole-cell staining and imaged every minute for 30 min after addition of 100 μM L^3Pt (green fluorescence) to the cell medium. Images acquired at time points of 0, 5, 15, and 30 min are shown.

show good activities in the cisplatin-resistant cell line A2780cisR, with lower resistance factors than cisplatin. The results of the ultrastructural analysis seem to be in agreement with the viability and cellular uptake studies, revealing that the high cytotoxic potency found for L²Pt can be justified in terms of a different mode of action from L³Pt or *cis*-DDP. Unlike L³Pt, L²Pt accumulates more in the cytoplasm than in the nuclei of ovarian cancer cells and shows a lower affinity for DNA with a less probable involvement of intercalative binding. The enhanced cytotoxicity of L²Pt might therefore be due to interaction with biological target(s) other than nuclear DNA. Most probably, the presence of the anthracenyl fragment increases the lipophilicity of L²Pt, enabling easier entrance into the cell than for the other Pt^{II} complexes evaluated in this study. Once inside the cell, L²Pt is retained essentially in the cytoplasm, and its action might involve direct interaction with a cytoplasmic target such as the mitochondria. Interestingly, a significant part of the clinical activity of cisplatin against neck and head cancers has been attributed to the interference of the drug with mitochondrial components and function.^[37–39] Further studies to elucidate the role of the interaction with mitochondria in the cytotoxic activity of the anthracenyl-containing complex L²Pt are underway. Mitochondrial depolarization with alteration of the mitochondrial potential gradient ($\Delta\psi$) might be involved in the mechanism of action of this compound.

Experimental Section

All chemicals (analytical grade) were obtained from Aldrich, except for K₂PtCl₄, which was from Alfa Aesar (a Johnson Matthey Company, Karlsruhe, Germany), and used as received. The compounds L¹Pt (L¹ = *N*-(2-(3,5-dimethyl-1*H*-pyrazol-1-yl)ethyl)ethane-1,2-diamine)^[7] 9-(3-aminopropyl)anthracene (1)^[11–14] and *tert*-butyl *N*-(2-((*tert*-butoxy)carbonyl)(2-(4-(2-(2,5-dioxopyrrolidin-1-yl)-2-oxoethyl)-3,5-dimethylpyrazol-1-yl)ethyl)amino)ethyl)carbamate (3)^[15] were prepared as reported elsewhere.

The purities of the Pt^{II} complexes were assessed by elemental analysis (C, H, N) and determination of Pt content by inductively coupled plasma-optical emission spectroscopy (ICP-OES). Elemental analyses were carried out with a EA3000 CHN Elemental Analyzer (EuroVector, Milano, Italy). Platinum was quantified with the aid of a Spectro Genesis ICP-OES spectrometer (Spectro Analytical Instruments, Kleve, Germany) fitted with a crossflow nebulizer. For quantification of platinum concentrations the Pt 299.797 line was selected. A platinum standard stock solution of 1000 mg L⁻¹ was diluted in nitric acid (1.0%, *v/v*) to prepare calibration standards. The elemental analyses and Pt content were within $\pm 0.4\%$ absolute of the theoretical value (except for complex L³Pt).

The multinuclear NMR spectra were measured with a JEOL Eclipse Plus instrument operating at 400 MHz (¹H), 100.5 MHz (¹³C), and 85.9 MHz (¹⁹⁵Pt with a spectral window of 2000 ppm). ¹H and ¹³C NMR chemical shifts are reported in parts per million (ppm) referenced to solvent resonances. ¹⁹⁵Pt NMR spectra were recorded with use of a solution of K₂[PtCl₄] in saturated aqueous KCl as the external reference. The shift for K₂PtCl₄ was adjusted to -1628 ppm from Na₂PtCl₆ ($\delta = 0$ ppm).

ESI-MS was performed with a Micromass ZMD mass spectrometer (Micromass, Manchester, UK). Typically, a diluted solution of the compound in methanol (with 2% of the suitable co-solvent) was

delivered directly to the spectrometer source at 0.01 mL min⁻¹ by Hamilton microsyringe controlled by a single-syringe infusion pump. The nebulizer tip operated at 3000–3500 V and 150 °C, with nitrogen used both as a drying and a nebulizing gas. The cone voltage was usually 30 V. Peaks were assigned on the basis of the *m/z* values and of the simulated isotope distribution patterns.

Ion chromatography was performed with a Dionex DX500 ion chromatograph (Dionex Corp., Sunnyvale, CA, USA) fitted with a Dionex GP40 Gradient Pump and a Dionex ED40 Electrochemical Detector. An anion-exchange Dionex IonPac AS14A (4 × 250 mm) column with an AG14A pre-column was used as stationary phase, and a carbonate (8 mM)/bicarbonate (1 mM) buffer was used as eluent [flow = 1 mL min⁻¹; H₂SO₄ (100 mM) was used as chemical suppressor].

Synthesis of the tridentate pz*NN ligands

10-(3-Aminopropyl)-3,6-bis(dimethylamino)acridinium iodide (2): Solid KI (3.13 g, 18.8 mmol) was added to a solution of *N*-(3-bromopropyl)phthalimide (3.00 g, 11.2 mmol) in pre-dried acetone (60 mL), and the mixture was heated at reflux for 48 h. The mixture was filtered and the filtrate was dried under reduce pressure to afford crude *N*-(3-iodopropyl)phthalimide as a yellow solid (3.47 g, 11 mmol, $\eta = 98\%$). ¹H NMR (300 MHz; CDCl₃): $\delta = 7.83$ (t, 2H; H-Phtha), 7.70 (t, 2H; H-Phtha), 3.75 (t, 2H; H-1), 3.14 (t, 2H; H-3), 2.22 ppm (m, 2H; H-2).

N-(3-Iodopropyl)phthalimide (1.00 g, 3.18 mmol) was dissolved in *p*-xylene (25 mL). Acridine orange (0.42 g, 1.59 mmol) and NaHCO₃ were added slowly to the *p*-xylene solution, and the resulting mixture was heated at reflux for 72 h. The formed red precipitate of 3,6-bis(dimethylamino)-10-(3-(1,3-dioxoisindolin-2-yl)propyl)acridinium iodide was filtered, washed with diethyl ether, and dried under vacuum (0.85 g, 1.45 mmol, $\eta = 91\%$). ¹H NMR (300 MHz; CDCl₃): $\delta = 8.64$ (s, 1H; H22), 7.82 (d, 2H; H21 and H25), 7.75 (d, 4H; H-Phthal), 6.98 (d, 2H; H20 and H26), 6.53 (s, 2H, H16 and H30), 4.90 (t, 2H; H14), 4.12 (t, 2H; H12), 3.21 (s, 12H; H18, H19, H28, and H29), 2.35 ppm (m, 2H; H13).

Hydrazine monohydrate (1.7 mL, 33.47 mmol) was added to a suspension of 3,6-bis(dimethylamino)-10-(3-(1,3-dioxoisindolin-2-yl)propyl)acridinium iodide (2.16 g, 3.72 mmol) in dry methanol (150 mL), and the mixture was heated at reflux for 42 h. After addition of concentrated HCl (37%, 5 mL), a white solid (phthalic acid hydrazide) precipitated. After filtration, the pH of the solution was adjusted to about 9 with NaOH (3 M). The reaction mixture was extracted with chloroform (3 × 50 mL), and the combined organic phases were dried over MgSO₄, concentrated under reduced pressure, and purified by Al₂O₃ column chromatography (eluent: MeOH (100–90%)/NH₃ (0–10%)). 10-(3-Aminopropyl)-3,6-bis(dimethylamino)acridinium iodide was obtained as a red solid after removal of the solvent from the collected fractions (0.22 g, 0.62 mmol, $\eta = 17\%$). ¹H NMR (300 MHz; CD₃OD): $\delta = 8.46$ (s, 1H; H23), 7.73 (d, ²*J* = 9.9 Hz, 2H; H21 and H25), 7.11 (d, ²*J* = 7.5 Hz, 2H; H20 and H26), 6.59 (s, 2H; H16 and H30), 4.66 (t, ³*J* = 8.1 Hz, 2H; H14), 3.27 (s, 4H; H12), 3.01 (s, 12H; H18, H19, H28, and H29), 2.06 ppm (m, 2H; H13).

Synthesis of 10-(4-(2-(1-(2-(2-aminoethylamino)ethyl)-3,5-dimethyl-1*H*-pyrazol-4-ylacetamido)propyl)anthracene (L²): A mixture of 1 (0.066 g, 0.28 mmol) and *N,N*-diisopropylethylamine (DIPEA; 0.1 mL, 0.56 mmol) in dry CH₂Cl₂ was added dropwise under nitrogen and at room temperature to a solution of 3 (0.15 g, 0.28 mmol) in dry CH₂Cl₂ (5 mL), and the resulting solution was stirred for 48 h. The formed precipitate was filtered off, and the fil-

trate was washed with water (3 × 20 mL). The organic phase was dried over MgSO₄ and concentrated under reduced pressure, giving the BOC-protected precursor of **L**² as a yellowish solid. This yellow solid (0.15 g, 0.26 mmol) was dissolved in MeOH (5 mL), and HCl 37% (1 mL) was added to the methanolic solution dropwise at 0 °C. The mixture was stirred at room temperature for 24 h. The pH was then adjusted to 12 with aqueous NaOH (3 M) and the mixture was extracted with chloroform (3 × 20 mL). The combined organic phases were dried over MgSO₄ and concentrated under reduced pressure to give **L**² as a pale solid (0.076 g, 0.17 mmol, η = 65%). ¹H NMR (300 MHz; CDCl₃): δ = 8.31 (s, 1H; H22), 8.14 (d, ²J = 8.7 Hz, 2H; H20 and H24), 7.98 (d, ²J = 8.1 Hz, 2H; H17 and H27), 7.45 (m, 2H; H18, H19, H25, and H26), 5.79 (s, 1H; NH), 4.06 (t, ³J = 6.0 Hz, 2H; H4), 3.56 (t, ³J = 8.1 Hz, 2H; H12), 3.41 (m, 2H; H3), 3.29 (s, 2H; H10), 2.96 (t, ³J = 6.0 Hz, 2H; H14), 2.63–2.56 (m, 4H; H2 and H1), 2.14 (s, 6H; H8 and H9), 1.91 ppm (m, 2H; H13); ¹³C NMR (300 MHz; CDCl₃): δ = 173.4 (C11), 146.7 (C5 or C7), 143.5 (C22), 140.0 (C16 and C28), 139.9 (C7 or C5), 131.1 (C21 and C23), 129.3 (C20 and C24), 126.3 (C17 and C27), 110.9 (C6), 101.3 (C18, C19, C25, and C26), 48.4 (C4), 46.9 (C2 and C3), 39.7 (C1), 38.1 (C12), 33.0 (C14), 32.6 (C10), 29.3 (C13), 11.9 (C9), 10.1 ppm (C8); ESI-MS (MeOH): calcd (%) for C₂₈H₃₆N₅O⁺: 458.29 (100.00); found: 458.2 (100.00) [M+H]⁺.

10-(4-(2-(1-(2-(2-Aminoethylamino)ethyl)-3,5-dimethyl-1H-pyrazol-4-ylacetamido)propyl)-3,6-bis(dimethylamino)acridinium (**L**³): Compound **3** (0.22 g, 0.62 mmol) was dissolved in dry DMF (30 mL), and the mixture was stirred for 1 h under nitrogen. DIPEA (80 μL, mmol) was then added to the suspension, followed by the addition of compound **1** (0.11, 0.21 mmol) dissolved in dry DMF (30 mL). After 94 h stirring at room temperature, the solvent was evaporated and a red oil was obtained. The red oil (0.54 g, 0.62 mmol) was dissolved in MeOH (5 mL) and cooled to 0 °C in an ice bath, and HCl (37%, 3 mL) was added. The reaction mixture was stirred at room temperature. After 24 h, the pH was adjusted to 12 with aqueous NaOH (3 M), the reaction mixture was extracted with chloroform (3 × 20 mL), and the combined organic phases were dried over MgSO₄ and concentrated under reduced pressure. Ligand **L**³ was then obtained as a red solid after purification by Al₂O₃ column chromatography (eluent: MeOH/NH₃ 100:0–95:5). (0.18 g, 0.27 mmol, η = 44%). ¹H NMR (300 MHz; MeOD): δ = 8.50 (s, 1H; H23), 7.79 (d, ²J = 9.3 Hz, 2H; H21 and H25), 7.14 (d, ²J = 9.3 Hz, 2H; H20 and H26), 6.48 (s, 2H; H16 and H27), 4.60 (t, ³J = 9.0 Hz, 2H; H4), 4.10 (t, ³J = 6.0 Hz, 2H; H14), 3.53 (t, ³J = 6.3 Hz, 2H; H12), 3.36 (s, 2H; H10), 3.34–3.29 (m, 2H; H18, H19, H28, and H29), 2.99 (t, ³J = 6.3 Hz, 2H; H3), 2.82 (t, ³J = 6.0 Hz, 2H; H13), 2.26 (m, 4H; H1 and H2), 2.16 ppm (m, 6H; H8 and H9); ¹³C NMR (300 MHz; MeOD): δ = 174.3 (C11), 157.1 (C17 and C27), 147.8 (C5 or C7), 144.0 (C23), 143.6 (C15 and C31), 139.9 (C7 or C5), 134.3 (C21 and C25), 118.1 (C22 and C24), 115.0 (C16 and C30), 111.4 (C6), 93.3 (C20 and C26), 48.4 (C4 and C14), 46.9 (C2 and C3), 41.1 (C18, C19, C28, and C29), 40.1 (C1), 38.3 (C12), 31.8 (C10), 27.0 (C13), 12.0 (C9), 9.2 ppm (C8). ESI-MS (MeOH): calcd (%) for C₃₁H₄₅N₈O⁺: 545.37 (100.00); found: 545.3 (100.00) [M]⁺, 273.1 (100.00) [M+H]²⁺/2.

Synthesis of the Pt^{II} complexes (Dhara Method)

Synthesis of the iodido complex L²Pt^{II}: K₂[PtCl₄] (0.188 g, 0.452 mmol) in water (5 mL) was treated at room temperature with a solution of KI (0.750 g, 4.518 mmol) in the same solvent (2 mL). The solution was stirred for 20 min and then treated with **L**² (0.188 g, 0.411 mmol) in DMF (2 mL). After 24 h, **L²Pt^{II}** was separated as a yellow precipitate by centrifugation, washed with water, and dried under vacuum. Yield: 0.231 g, 0.255 mmol, 62% from **L**².

¹H NMR ([D₇]DMF): δ = 8.53 (m, 1H; H22), 8.39 (m, 2H; H17 and H27), 8.23 (m, 1H; C(O)NH), 8.13 (m, 2H; H20 and H24), 7.56 (m, 4H; H18, H19, H25, and H26), 7.22 (m, 1H; NH), 5.81 (m, 2H; NH₂), 4.92 (m, 1H; H_{4ax}), 4.58 (m, 1H; H_{4eq}), 3.71 (m, 2H; H12), 3.46 (m, 4H; H10 and H14), 3.35–3.20 (m, 2H; H3), 2.96 (m, 2H; H2), 2.80 (m, 2H; H1), 2.51 (s, 6H; H8 or H9), 2.50 (s, 6H; H8 or H9), 1.98 ppm (m, 2H; H13); ¹³C NMR ([D₇]DMF): δ = 169.61 (C11), 151.14 (C5 or C7), 141.75 (C5 or C7), 134.70 (C15), 131.87 (C21 and C23), 129.65 (C16 and C28), 129.35 (C20 and C24), 125.98 (C22), 125.88 (C18 and C26), 125.22 (C19 and C25), 124.52 (C17 and C27), 113.62 (C6), 57.38 (C2), 50.54 (C3), 49.33 (C1 and C4), 39.55 (C14), 31.48 (C13), 30.65 (C10), 25.27 (C12), 15.56 (C8 or C9), 9.78 ppm (C8 or C9); ¹⁹⁵Pt NMR ([D₇]DMF): –3113 ppm. ESI-MS (MeOH, 2% DMF): calcd (%) for C₂₈H₃₅IN₅O⁺: 779.15 (100.00); found: 779.44 (100.00) [M–I]⁺.

Synthesis of the chlorido complex L²Pt^{II} [PtCl(L²)]Cl: Complex **L²Pt^{II}** (0.212 g, 0.234 mmol) in water (8 mL) was added to a solution of AgNO₃ (0.122 g, 0.718 mmol) in water (10 mL) and the mixture was stirred in the dark at 50 °C. After 4 h, KCl (0.104 g, 1.397 mmol) was added at room temperature. The solution was stirred at room temperature for 20 h. After this, the mixture was centrifuged and then filtered to remove any insoluble material. The filtrate was cooled at –20 °C and lyophilized. The yellow residue was washed with cold water and then dried under nitrogen flow and in vacuo. Complex **L²Pt^{II}** was dissolved in water and added to a suspension of anion-exchange resin (Amberlite IRA-400, Rohm&Haas Co. in chloride form) in water. After 30 min the suspension was filtered, and the filtrate was frozen and lyophilized. The residue was washed with cold water to remove excess KCl. Yield: 0.051 g, 30% from **L²Pt^{II}**. ¹H NMR ([D₆]acetone): δ = 8.42 (s, 1H; H22), 8.35 (d, ³J = 8.6 Hz, 2H; H17 and H27), 8.05 (d, ³J = 8.6 Hz, 2H; H20 and H24), 7.63 (brs, 1H; C(O)NH), 7.60–7.40 (m, 4H; H18, H19, H25, and H26), 5.45–5.20 (m, 3H; NH and NH₂), 4.90 (m, ²J = 15.1 Hz, ³J_{ax} = 12.0 Hz, ³J_{ax} = 2.6 Hz, 1H; H_{4ax}), 4.47 (m, ²J = 15.1 Hz, ³J_{ax} = 3.0 Hz, 1H; H_{4eq}), 3.63 (m, 2H; H12), 3.53 (m, 2H; H14), 3.36 (s, 2H; H10), 3.35–3.28 (m, 2H; H3), 3.00–2.90 (m, 4H; H2 and H1), 2.45 (s, 3H; H8 or H9), 2.38 (s, 3H; H8 or H9), 2.05–1.90 ppm (m, 2H; H13); ¹³C NMR ([D₆]acetone): δ = 169.08 (C11), 150.94 (C5 or C7), 140.98 (C5 or C7), 134.84 (C15), 131.85 (C21), 129.62 (C3), 129.13 (C20 and C24), 125.68 (C18 and C26), 125.57 (C22), 124.98 (C19 and C25), 124.52 (C17 and C27), 112.75 (C6), 58.37 (C2 or C1), 50.52 (C3), 49.43 (C4), 47.45 (C2 or C1), 39.57 (C14), 31.38 (C13), 30.80 (C10), 25.34 (C12), 11.70 (C8 or C9), 9.43 ppm (C8 or C9); ¹⁹⁵Pt NMR ([D₆]acetone): –2632 ppm. ESI-MS (MeOH): calcd (%) for C₂₈H₃₅ClN₅O⁺: 688.22 (100.00); found: 688.35 (100.00) [M–Cl]⁺.

Synthesis of iodido complex L³Pt^{II}: K₂[PtCl₄] (0.148 g, 0.357 mmol) in water (5 mL) was treated with a solution of KI (0.593 g, 3.570 mmol) in the same solvent (2 mL). The solution was stirred for a few minutes and then treated with a stoichiometric amount of **L**³ (0.235 g, 0.357 mmol) in water (5 mL). After 24 h of stirring at room temperature, **L³Pt^{II}** was separated as a red precipitate by centrifugation, washed with water, and dried under vacuum. Yield: 0.078 g (19%). ¹H NMR ([D₇]DMF): δ = 8.96 (s, 1H; H23), 8.30 (t, ³J = 5.5 Hz, 1H; C(O)NH), 8.09 (brd, ³J = 9.5 Hz, 2H; H21 and H25), 7.41 (dd, ⁴J = 2.0 Hz, ³J = 9.5 Hz, 2H; H20 and H26), 7.21 (m, 1H; NH), 6.85 (s, 2H; H16 and H30), 5.82 (m, 2H; NH₂), 4.93 (m, 3H; H_{4ax} and H12), 4.60 (d, ²J = 15.0 Hz, 1H; H_{4eq}), 3.67 (m, 2H; H14), 3.50 (s, 2H; H10), 3.41 (s, 12H, H18, H19, H28, and H29), 3.40–3.20 (m, 2H; H3), 3.05–2.90 (m, 2H; H2), 2.90–2.80 (m, 2H; H1), 2.47 (s, 3H; H8 or H9), 2.46 (s, 3H; H8 or H9), 2.28 ppm (m, 2H; H13); ¹³C NMR ([D₇]DMF): δ = 170.09 (C11), 156.14 (C5 or C7), 151.16 (C17), 143.35 (C15), 142.89 (C23), 141.79 (C5 or C7), 133.43 (C21 or C25), 117.28

(C22 or C24), 114.72 (C20 or C26), 113.36 (C6), 92.85 (C16 or C30), 57.41 (C2), 50.57 (C3), 49.36 (C1 and C4), 45.67 (C12), 40.42 (C18, C19, C28, and C29), 37.08 (C14), 30.83 (C10), 26.29 (C13), 15.64 (C8 or C9), 9.91 ppm (C8 or C9); ¹⁹⁵Pt NMR ([D₇]DMF): −3112 ppm; ESI-MS (MeOH, 2% DMF): calcd (%) for C₃₁H₄₅IN₈OPt²⁺: 433.86 (100.00); found: 433.76 (100.00) [M−2I]²⁺/2.

Synthesis of the chlorido complex L³Pt {[PtCl(L³)]Cl_{0.04}(NO₃)_{0.96}}: Complex L³Pt' (0.078 g, 0.070 mmol) in water (8 mL) was added to a solution of AgNO₃ (0.036 g, 0.209 mmol) in water (8 mL) and the resulting mixture was stirred in the dark for 4 h at 50 °C. The mixture was centrifuged to remove AgI, and then KCl (0.026 g, 0.350 mmol) was added to the filtrate. The solution was stirred at room temperature for 20 h. After stirring, the mixture was centrifuged and filtered to remove solid AgCl and AgI. The filtrate was concentrated under reduced pressure and then cooled at 4 °C to induce the precipitation of the red product. The mixture was centrifuged and the precipitate was separated, washed with cold water, and dried under vacuum. Yield: 0.025 g, 40% as dinitrate form from L³Pt'. ¹H NMR (CD₃OD): δ = 8.51 (s, 1H; H23), 7.80 (d, ²J = 9.1 Hz, 2H; H21 and H25), 7.18 (d, ²J = 9.1 Hz, 2H; H20 and H26), 6.89 (m, 1H; NH), 6.56 (s, 2H; H16 and H30), 5.60 (m, 2H; NH2), 4.90–4.80 (m, 1H; H_{ax}), 4.61 (m, 2H; H12), 4.38 (m, 1H; H_{eq}), 3.51 (m, 2H; H14), 3.38 (s, 2H; H10), 3.28 (s, 12H; H18, H19, H28, and H29), 3.10–2.80 (m, 4H; H3 and H2), 2.75–2.55 (m, 2H; H1), 2.45 (s, 3H; H8 or H9), 2.34 (s, 3H; H8 or H9), 2.20–2.10 ppm (m, 2H; H13); ¹³C NMR (CD₃OD): δ = 174.00 (C11), 157.36 (C5 or C7), 152.42 (C17), 144.20 (C15), 143.92 (C23), 142.69 (C5 or C7), 134.34 (C21 and C25), 118.37 (C22 and C24), 115.44 (C20 and C26), 113.69 (C6), 93.45 (C16 and C30), 59.56 (C2), 51.63 (C3), 50.20 (C4), 47.63 (C1), 46.60 (C12), 40.92 (C18, C19, C28 and C29), 38.44 (C14), 31.50 (C10), 26.94 (C13), 12.92 (C8 or C9), 10.28 ppm (C8 or C9); ¹⁹⁵Pt NMR (CD₃OD): −2655 ppm; ESI-MS (MeOH): calcd (%) for C₃₁H₄₅ClN₈OPt²⁺: 388.14 (100.00); found: 387.67 (100.00) [M−2NO₃]⁺/2.

DNA interaction: The DNA interaction was evaluated by monitoring the mobilities of supercoiled plasmid DNA (covalently closed circular, ccc) and open circular DNA (oc), as previously described.^[7] The plasmid DNA used was ϕX174 plasmid DNA (Promega). Each reaction mixture was prepared by adding water (6 μL), supercoiled DNA (2 μL, 200 ng), stock Na₂HPO₄/HCl buffer solution (pH 7.2, 100 mM, 2 μL), and the solution of the complex (10 μL). The final reaction volume was 20 μL, the final buffer concentration was 10 mM, and the final metal concentration varied from 0.1 to 100 μM, corresponding to r_i (input molar ratio of Pt/nucleotide) of 0.03 to 3.33. Samples were typically incubated for 24 h at 37 °C, in the dark. After incubation, DNA loading buffer (bromophenol blue (0.25%), xylene cyanol (0.25%), glycerol in water (30%), Applchem, 4 μL) was added to each tube and the sample was loaded onto an agarose gel (0.8%) in TAE buffer [Tris (40 mM), acetic acid (20 mM), EDTA (1 mM), pH 8.0]. Controls of non-incubated plasmid and of plasmid incubated with DMSO were loaded on each run. The electrophoresis was carried out for 3.5 h at 90 V.

In the case of the studies with chloroquine, the reaction mixture was prepared as previously described but with a final metal complex concentration of 5 μM (r_i = 0.17). The samples were incubated for 24 h at 37 °C. After the addition of DNA loading buffer, the samples were loaded on to an agarose gel (0.8%) in TAE buffer, and the electrophoresis was performed for 16 h at 20 V in TAE buffer containing chloroquine (1.25 μg mL^{−1}, in order to resolve DNA topoisomers). The gels were then stained with TAE buffer containing ethidium bromide (0.5 μg mL^{−1}). Bands were visualized under UV light, and images were captured with an AlphamagerEP (Alpha

Innotech). All samples in each figure were obtained from the same run.

Cytotoxicities: Human ovarian carcinoma cells (A2780 and A2780cisR) were grown in RPMI 1640 medium supplemented with fetal bovine serum (FBS, 10%) and L-glutamine (2 mM, both from Invitrogen) under a humidified atmosphere at 37 °C (5% CO₂).

Cytotoxic activity was evaluated by MTT assay.^[11] A2780 and A2780cisR cells were plated on 96-well plates at a density of 8–20 × 10³ cells per well with medium (200 μL) and incubated overnight. After attachment to the well surface, cells were incubated with various concentrations of the complexes freshly dissolved in DMSO (except for cisplatin, which was solubilized in water) and diluted in the culture medium (DMSO final concentration < 1%) for 24 or 72 h at 37 °C. At the end of the incubation period, the compounds were removed, and the cells were incubated with MTT solution (0.5 mg mL^{−1}, 200 μL). After 3–4 h at 37 °C/5% CO₂, the medium was removed and the purple formazan crystals formed inside the cells were dissolved in DMSO (200 μL) by thorough shaking. The cellular viability was evaluated by measurement of the absorbance at 570 nm with a plate spectrophotometer (PowerWave Xs, Bio-Tek Instruments, Winooski, VT, USA). The cytotoxic effects of Pt complexes were quantitated by calculating the IC₅₀ values, based on nonlinear regression analysis of dose-response data. For comparison, the cytotoxicity of cisplatin was evaluated under the same experimental conditions. Each compound was tested in at least two independent studies with six replicates.

The evaluation of the combined effect of the alkylating Pt moiety and its intercalating ligand was performed by comparing their cytotoxicity data by the combination index (CI) methodology.^[35–36] The CI values for compounds L²Pt and L³Pt were calculated for 50% residual viability according to the model of interaction for two mutually non-exclusive drugs:

$$CI = \frac{C_A}{IC_{50,A}} + \frac{C_B}{IC_{50,B}} + \frac{C_A \times C_B}{IC_{50,A} \times IC_{50,B}}$$

where IC_{50,A} and IC_{50,B} are the concentrations for single agents A and B, respectively, needed to achieve 50% residual viability, and C_A and C_B are the concentrations of drugs A and B used in combination to achieve the same effect.

Uptake by ICP-MS: ICP-MS analyses were carried out with a Thermo X-Series Quadrupole ICP-MS instrument (Thermo Scientific) by a method previously described by us.^[7] Briefly, cells were exposed to Pt complexes (10 μM) for 3 and 24 h at 37 °C and were then washed with cold PBS and centrifuged to obtain a cellular pellet. The cytosolic and nuclear fractions were separated by using a commercial kit (NE-PER from Pierce-Thermo Scientific), according to the manufacturer's recommendations. The concentrations of Pt^{II} in the different fractions were measured after digestion. Briefly, samples were digested with ultrapure HNO₃ (65%), H₂O₂, and H₃PO₄ in a closed pressurized microwave digestion unit (Mars5, CEM) with medium pressure HP500 vessels and then diluted in ultrapure water to obtain 2.0% (v/v) nitric acid. The instrument was tuned with a multielement ICP-MS 71 C standard solution (Inorganic Venture). Indium (¹¹⁵In) at 10 μg mL^{−1} was used as internal standard.

Uptake by fluorescence microscopy: Cellular uptake of L³Pt was visualized by time-lapse confocal microscopy imaging of live A2780 cells. Briefly, cells in medium (ca. 105 cells mL^{−1}) were seeded on sterile 35 mm Petri dishes (MatTek, Ashland, MA, USA). After 24 h incubation at 37 °C, cells were labeled with DHE (Molec-

ular Probes, Eugene, OR, USA) at $1 \mu\text{g mL}^{-1}$ for 15 min at 37°C . DHE freely permeates cell membranes and inside the cell is oxidized to ethidium bromide (red fluorescence).

After labeling, the cells were washed and maintained in DMEM/F12 for live imaging experiments. Cells were imaged with a Zeiss LSM 510 META inverted laser scanning confocal microscope (Carl Zeiss, Germany) fitted with a large incubator for 37°C (Pecon, Germany) with use of a PlanApochromat 963/1.4 oil-immersion objective. Ethidium bromide fluorescence was detected by use of the 514 nm laser line of an argon laser (45 mW nominal output) and a 615 nm long-pass filter. The fluorescence of compound **L³Pt** was detected by use of the 488 nm laser line of the same Ar laser and a 500–550 nm band-pass filter. The pinhole aperture was adjusted in both channels to achieve the same optical slice thickness ($1 \mu\text{m}$). After addition of the complex to the cells ($100 \mu\text{M}$, final concentration) sequential images in both green (**L³Pt**) and red (ethidium bromide) channels were acquired every minute over a 30 min time period.

Ultrastructural analysis: A2780 cells at approximately 70% confluence were treated with **L²Pt** and **L³Pt** ($20 \mu\text{M}$) at 37°C for 2 h. After incubation, the culture media was replaced by primary fixative (5 mL) consisting of glutaraldehyde (3%) in sodium cacodylate buffer (pH 7.3, 0.1 M). After primary fixation for 2 h at 4°C , cells were scraped, pelleted, and embedded in agar (2%) for further processing. The samples were washed in cacodylate buffer and secondarily fixed for 3 h in osmium tetroxide (1%) in sodium cacodylate buffer (pH 7.3, 0.1 M). Then samples were washed in acetate buffer (pH 5.0, 0.1 M) and further fixed in uranyl acetate (0.5%) in the same buffer for 1 h. Dehydration was carried out with increasing concentrations of ethanol. After passage through propylene oxide, the samples were embedded in Epon-Araldite, with use of SPI-Pon as an Epon 812 substitute. Thin sections were made with glass or diamond knives and stained with aqueous uranyl acetate (2%) and Reynold's lead citrate. The stained sections were studied and photographed with a JEOL 100-SX electron microscope.

Acknowledgements

The authors would like to thank the Fundação para a Ciência e Tecnologia (FCT) for the postdoctoral research grant (SFRH/BPD/29564/2006), as well as FEDER and FCT for financial support (PTDC/QUI/66813/2006). The research was carried out within the framework of the European Cooperation COST Action CM1105 (Functional Metal Complexes that Bind to Biomolecules) and Consorzio Interuniversitario di Ricerca in Chimica dei Metalli nei Sistemi Biologici (CIRCMSB, Bari, Italy). Joaquim Marçalo is acknowledged for the ESI-MS analyses, which were run with a QITMS instrument acquired with the support of the Programa Nacional de Reequipamento Científico (Contract REDE/1503/REM/2005-ITN) of the Fundação para a Ciência e a Tecnologia and is part of RNEM (Rede Nacional de Espectrometria de Massa). The authors thank Dr. Eugénio Soares of LCA-Aveiro University for the ICP-MS platinum uptake studies.

Keywords: antitumor agents • cytotoxicity • DNA binding • platinum complexes • pyrazolyl ligands

- [1] D. Wang, S. J. Lippard, *Nat. Rev. Drug Discovery* **2005**, *4*, 307–320.
- [2] K. S. Lovejoy, S. J. Lippard, *Dalton Trans.* **2009**, 10651–10659.
- [3] S. v. Zutphen, J. Reedijk, *Coord. Chem. Rev.* **2005**, *249*, 2845–2853.
- [4] S. Komeda, *Metallomics* **2011**, *3*, 650–655.
- [5] R. A. Alderden, H. R. Mellor, S. Modok, T. W. Hambley, R. Callaghan, *Biochem. Pharmacol.* **2006**, *71*, 1136–1145.
- [6] R. M. Whan, B. A. Messerle, T. W. Hambley, *Dalton Trans.* **2009**, 932–939.
- [7] C. Francisco, S. Gama, F. Mendes, F. Marques, I. Cordeiro dos Santos, A. Paulo, I. Santos, J. Coimbra, E. Gabano, M. Ravera, *Dalton Trans.* **2011**, *40*, 5781–5792.
- [8] R. F. Vitor, I. Correia, M. Videira, F. Marques, A. Paulo, J. Costa Pessoa, G. Viola, G. G. Martins, I. Santos, *ChemBioChem* **2008**, *9*, 131–142.
- [9] R. F. Vitor, T. Esteves, F. Marques, P. Raposo, A. Paulo, S. Rodrigues, J. Rueff, S. Casimiro, L. Costa, I. Santos, *Cancer Biother. Radiopharm.* **2009**, *24*, 551–563.
- [10] T. Esteves, C. Xavier, S. Gama, F. Mendes, P. D. Raposo, F. Marques, A. Paulo, J. C. Pessoa, J. Rino, G. Viola, I. Santos, *Org. Biomol. Chem.* **2010**, *8*, 4104–4116.
- [11] C. V. Kumar, E. H. A. Punzalan, W. B. Tan, *Tetrahedron* **2000**, *56*, 7027–7040.
- [12] R. A. Hann, *J. Chem. Soc. Perkin Trans. 1* **1974**, 1379–1380.
- [13] R. A. Rhodes, D. W. Boykin, *Synth. Commun.* **1988**, *18*, 681–687.
- [14] L. H. Amundsen, L. S. Nelson, *J. Am. Chem. Soc.* **1951**, *73*, 242–244.
- [15] C. Moura, T. Esteves, L. Gano, P. D. Raposo, A. Paulo, I. Santos, *New J. Chem.* **2010**, *34*, 2564–2578.
- [16] N. G. Di Masi, F. P. Intini, C. Pacifico, L. Maresca, G. Natile, *Inorg. Chim. Acta* **2000**, *310*, 27–33.
- [17] G. W. Watt, W. A. Cude, *Inorg. Chem.* **1968**, *7*, 335–338.
- [18] R. C. Harrison, C. A. McAuliffe, A. M. Zaki, *Inorg. Chim. Acta* **1980**, *46*, L15–L16.
- [19] F. D. Rochon, L. M. Gruia, *Inorg. Chim. Acta* **2000**, *306*, 193–204.
- [20] S. C. Dhara, *Indian J. Chem.* **1970**, *8*, 193–194.
- [21] J. K. Beattie, L. H. Novak, *J. Am. Chem. Soc.* **1971**, *93*, 620–624.
- [22] J. K. Beattie, H. Elsbernd, *J. Am. Chem. Soc.* **1970**, *92*, 1946–1948.
- [23] J. K. Beattie, *Acc. Chem. Res.* **1971**, *4*, 253–259.
- [24] S. Aime, M. Botta, G. Ermondi, *Inorg. Chem.* **1992**, *31*, 4291–4299.
- [25] J. F. Desreux, *Inorg. Chem.* **1980**, *19*, 1319–1324.
- [26] L. H. Novak, J. K. Beattie, *Inorg. Chem.* **1971**, *10*, 2326–2328.
- [27] A. Navarro-Vázquez, J. C. Cobas, J. Sardina, *J. Chem. Inf. Comput. Sci.* **2004**, *44*, 1680–1685.
- [28] C. Altona in *Encyclopedia of Magnetic Resonance*, Wiley, **2007**; DOI: 10.1002/9780470034590.emrstm0587.
- [29] M. V. Keck, S. J. Lippard, *J. Am. Chem. Soc.* **1992**, *114*, 3386–3390.
- [30] G. Cohen, W. Bauer, J. Barton, S. Lippard, *Science* **1979**, *203*, 1014–1016.
- [31] W. M. Scovell, F. Collart, *Nucleic Acids Res.* **1985**, *13*, 2881–2895.
- [32] S. F. Bellon, J. H. Coleman, S. J. Lippard, *Biochemistry* **1991**, *30*, 8026–8035.
- [33] S. Moradell, J. Lorenzo, A. Rovira, M. S. Robillard, F. X. Avilés, V. Moreno, R. de Llorens, M. A. Martínez, J. Reedijk, A. Llobet, *J. Inorg. Biochem.* **2003**, *96*, 493–502.
- [34] J. M. Pérez, I. López-Solera, E. I. Montero, M. F. Braña, C. Alonso, S. P. Robinson, C. Navarro-Ranninger, *J. Med. Chem.* **1999**, *42*, 5482–5486.
- [35] T.-C. Chou, P. Talalay, *Adv. Enzyme Regul.* **1984**, *22*, 27–55.
- [36] T.-C. Chou, *Cancer Res.* **2010**, *70*, 440–446.
- [37] E. Lindauer, E. Holler, *Biochem. Pharmacol.* **1996**, *52*, 7–14.
- [38] M. Groessl, O. Zava, P. J. Dyson, *Metallomics* **2011**, *3*, 591–599.
- [39] M. Crul, R. C. A. M. van Waardenburg, J. H. Beijnen, J. H. M. Schellens, *Cancer Treat. Rev.* **2002**, *28*, 291–303.

Received: July 16, 2012

Published online on October 4, 2012